



HAL
open science

Spatial and temporal evolution of ion and electron parameters in the plasma jet of a 30 W VAT

E Michaux, Stéphane Mazouffre, R Fritzsche

► **To cite this version:**

E Michaux, Stéphane Mazouffre, R Fritzsche. Spatial and temporal evolution of ion and electron parameters in the plasma jet of a 30 W VAT. 37th International Electric Propulsion Conference, Jun 2022, Cambridge, United States. hal-03797325

HAL Id: hal-03797325

<https://hal.science/hal-03797325>

Submitted on 4 Oct 2022

HAL is a multi-disciplinary open access archive for the deposit and dissemination of scientific research documents, whether they are published or not. The documents may come from teaching and research institutions in France or abroad, or from public or private research centers.

L'archive ouverte pluridisciplinaire **HAL**, est destinée au dépôt et à la diffusion de documents scientifiques de niveau recherche, publiés ou non, émanant des établissements d'enseignement et de recherche français ou étrangers, des laboratoires publics ou privés.

Spatial and temporal evolution of ion and electron parameters in the plasma jet of a 30W VAT

IEPC-2022-557

*Presented at the 37th International Electric Propulsion Conference
Massachusetts Institute of Technology, Cambridge, MA, USA
June 19-23, 2022*

E. Michaux¹, S. Mazouffre² and R. Fritzsche³
CNRS, ICARE Laboratory, 1C avenue de la recherche scientifique, 45071, Orléans, France

The plasma parameters temporal evolution of a 30 W-class Vacuum Arc Thruster equipped with a titanium (Ti) cathode is examined in the far-field region of the plasma jet. The change in the electron density, electron temperature and plasma potential during the short high-current pulse has been obtained by means of time-resolved Langmuir probe measurements. Probes were placed at 3 different locations on the thruster centerline: 20 cm, 25 cm and 30 cm. A time-of-flight technique has been used to determine the mean ion velocity in the plasma jet. We found a higher velocity than what is usually found in the literature for the same cathode material. Interestingly, combining all data allows to assess the ion mean electrical charge and its temporal behavior. The mean charge reaches 2+ a few μs after ignition. It decays quickly afterwards then decreases below 1 beyond 10 μs . Analysis of all the results support the idea of two distinct plasma discharge regimes.

I. Nomenclature

e	= elementary charge, 1.6×10^{-19} C
I_e	= electron current
j_i	= ion current density
n_e	= electron density
Q	= charge
T_e	= electron temperature
V_p	= plasma potential
v_i	= ion velocity
x	= position, distance

II. Introduction

Vacuum arc thrusters are space electric propulsion systems that operate with a solid propellant. A vacuum arc is triggered in the inter-electrode gap of the thruster, creating a metallic plasma from the vaporization and the ionization of the negative electrode material. Expansion and ejection of this highly ionized plasma at high velocities generates thrust [1]. As the ionization process occurs in a relatively small region and as the plasma is quasi-neutral [2], the vacuum arc thruster (VAT) shows inherent advantages for miniaturization. Unlike Hall Thrusters or Gridded Ion Engines, VATs do not require any external neutralizer. The consumption of a solid propellant through vaporization of the cathode itself suppresses the need of a propellant tank and any gas feeding system. This gives the ability to reduce the mass and size of the propulsion system. It also increases the reliability of the system, as less components are involved. Moreover,

¹Research Engineer, Electric Propulsion team, CNRS-ICARE, etienne.michaux@cnrs-orleans.fr

²Research Director, Head of the Electric Propulsion team, CNRS-ICARE, stephane.mazouffre@cnrs-orleans.fr

³Intern, Electric Propulsion team, CNRS-ICARE

vacuum arc discharges can be pulsed without losses in plasma production efficiency [3]. It is then possible to adapt the duty cycle of a VAT to match the electrical power available onboard a spacecraft.

However, VATs suffer from intrinsic shortcomings such as conductive metal deposition on the insulators, non homogeneous cathode erosion and cathode wear. This limits the performances as well as the lifetime of the thruster, resulting in a low total impulse. The unique physical conditions achieved in vacuum arcs are in fact an obstacle to the development of high-performance and reliable VATs. Despite several decades of research efforts, the vacuum arc physics still has some unknown surrounding it. At this stage, more experimental data is needed to better understand the formation of the arc, its dynamics and plasma acceleration mechanisms. In this way, codes and numerical simulations can be made more reliable, allowing new solutions and new architectures to be proposed. The final objective of all on-going studies is the increase in performances and lifetime of VATs in order to meet the requirements of a wide range of space missions.

As the inter-electrode region and the arc itself are difficult to probe, a first reasonable approach is to analyze properties of the plasma jet. The latter is indeed more accessible and less disturbed by insertion of instruments. In spite of a relatively easy access, the temporal evolution of fundamental plasma parameters like the electron density and temperature has been poorly investigated in the VAT plasma flow far from the source. In this contribution we present experiments performed with the PJP, a 30 W-class VAT equipped with a Titanium cathode. Similar works have been performed with the PJP thruster firing with a Ni-Cr cathode. More information can be found in reference [4]. The change in time of the electron density, the electron temperature and the plasma potential has been observed at the μs time scale during a typical current pulse. The three quantities have been determined through the analysis of time-varying current-voltage curves of a cylindrical Langmuir probe acquired over thousands of current pulses, as explained in the next sections. The ion velocity in the jet has also been assessed with a time-of-flight technique. This quantity is of great interest as it governs to a large extent the thrust level, the specific impulse as well as the thrust efficiency of a propulsive device. We also share and discuss ion current density measurements carried out with a Faraday cup far downstream the arc region. The current density is the main driver for the thrust, so it is a relevant quantity. By combining all experimental outcomes, we can assess the mean electrical charge of ions in the jet. The charge distribution in vacuum arcs has been the subject of numerous investigations as it is strongly related to the physical mechanisms at the origin of the arc formation and plasma ejection.

III. Experimental arrangement

A. PJP - H2020 version

The VAT under study is the Plasma Jet Pack (PJP) developed by the COMAT French company. This 30 W-class VAT generates a high DC current vacuum arc through the cyclic discharges of a capacitor bank. The cathode-anode voltage is continuously set to 250 V. A triggering system applies several kV for hundreds of ns on the cathode surface, initiating a plasma through an explosive process on a region called the cathodic spot [5]. The high voltage applied during the trigger phase initiates a breakdown by field emission [6] that is followed by a spark and then an arc. During VAT operation a thin metallic layer deposits on the insulator that separates the triggering system and the cathode. Ignition of the discharge is then easier as the breakdown occurs through the conductive layer. Note when the deposited layer becomes too thick it is more difficult to vaporize and the thruster no longer operates properly [1]. After the trigger is switched-off, the arc is forced to propagate to the anode through the existing metal vapor. This second arc discharge allow 1.5 to 2.5 kA to flow between the two electrodes on the current configuration. Measurements presented in this contribution have been obtained with a Titanium cathode and a copper anode. Moreover, the pulse frequency was set to 1 Hz to avoid thermal issues.

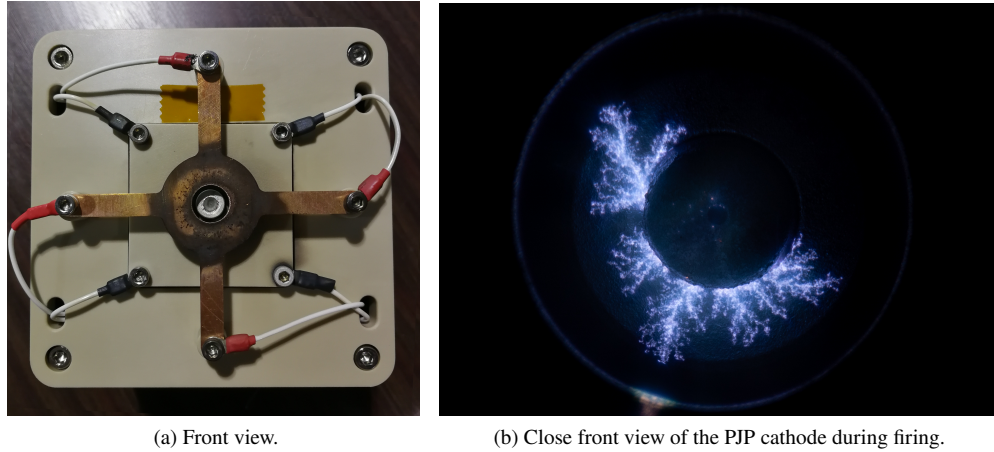


Fig. 1 Plasma Jet Pack thruster: front view (a) and plasma discharge in operation (b).

Fig. 1a shows the front view of a laboratory version of the PJP. The 4-legs electrode is here the annular copper anode. The cathode corresponds to the grey center-mounted cylinder. The latter is screwed onto a copper plate directly wired to the capacitor bank. The trigger electrode is a tiny metal tip placed exactly on the thruster axis. The laboratory version of the PJP can easily be disassembled and modified contrary to the flight version. The power unit is however the same for the two versions. The PJP target performances and characteristics are given in Table 1 for the inclined reader. Fig. 1b is a photograph of the arc discharge during a current pulse. As the exposure time of the camera is much longer than the VAT current pulse duration, the picture averages the arc dynamics and motion. The picture nevertheless exemplifies the complexity of the physical phenomena at the origin of thrust generation[7].

Table 1 PJP thruster target performances and characteristics.

Power	0-30	W
Thrust to power	10	$\mu\text{N/W}$
Average thrust @30 W	300	μN
Specific impulse	2,500	s
Total impulse	400	Ns
Overall mass	1	kg
Overall volume	1	U

B. Vacuum facility

Experiments have been performed in the EPIC-2 vacuum facility. This tank is a stainless steel cylinder 54 cm in radius and 104 cm in length, for an approximate capacity of 240 l. Two 2200 l/s (N_2) magnetically levitated STP-iS2207 from Edwards are placed on top of the chamber (see Fig. 2). Those pumps, evacuated through a 110 m^3/hr dry primary pump (Edwards GV110), permit to keep a background pressure of 10^{-6} mbar during thruster operation. The pressure is monitored with a Pfeiffer PBR260 Pirani/Payard-Alpert pressure gauge.

EPIC-2 is also equipped with several electrical feedthroughs, for both in-situ diagnostics and thruster power supply. Those feedthroughs are mostly composed of BNC or SubD connectors. Two Kodial (Borosilicate 7056) glass windows allow the visual inspection of the thruster.

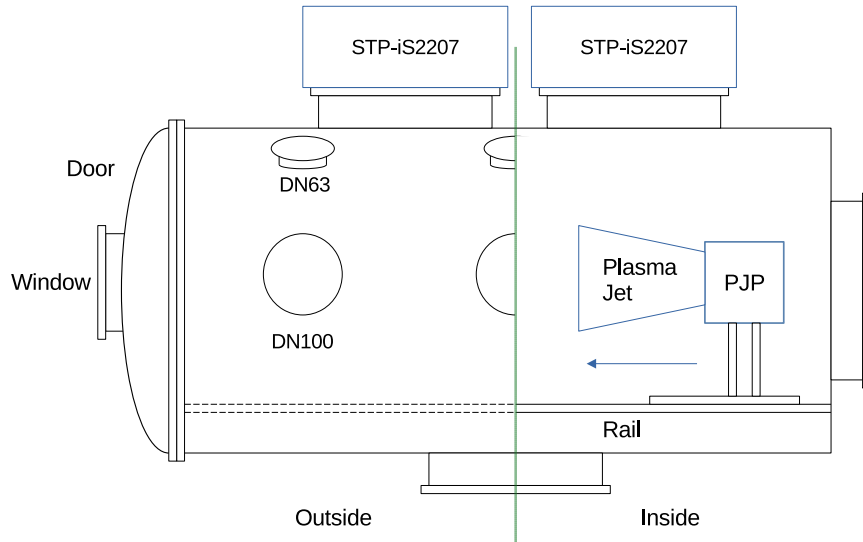


Fig. 2 Schematic of the EPIC 2 chamber

In EPIC 2, the PJP is placed on a plate, the latter is screwed on a rail. This mounting allows adjustments on the distance to the windows, depending on the experiment to be performed. For investigating the plasma plume by means of electrostatic probes, the PJP is placed far into the tank to let the plume expand as freely as possible.

C. Diagnostics

Because of the pulsed, brief and chaotic nature of the plasma discharge, obtaining shot-to-shot reproducible quantities is a hard task when investigating on the PJP plume. Consequently, we systematically focus here on a statistical approach of the observed phenomena. Electrostatic probes should then be connected to an instrument allowing the recording of current intensity values for each instant of the discharge. All the diagnostics presented hereafter have been read with a 1 GHz 12-bit HD06104A Teledyne LeCroy oscilloscope. The current probe used to measure the discharge current flowing on the PJP cathode line was a $50\ \Omega$ Stangenes 2-0.1WA, indicating an output ratio of 0.1 V/A. Fig. 3 shows the averaged discharge current profile obtained with 100 pulses. As it can be seen, the current rises up to more than 1.7 kA. A voltage divider with an output ratio of 1/100 has been therefore inserted between the current probe and the oscilloscope to avoid damaging the latter.

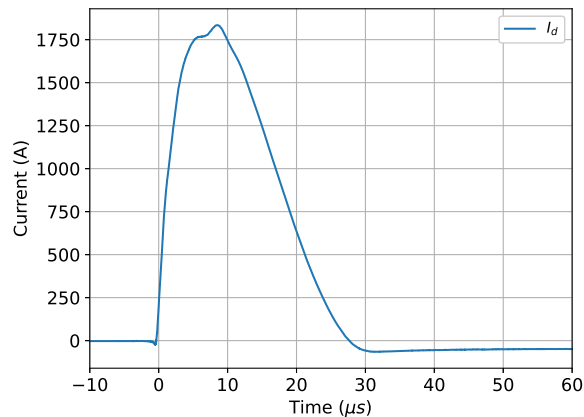


Fig. 3 Averaged PJP discharge current waveform (100 pulses, Ti cathode).

1. Langmuir probe and Faraday Cup

Langmuir probes (LP) are widely used diagnostics in plasma physics. LP theory permits to recover local physical quantities through analytical properties of Intensity vs Voltage (I-V) curves. Acquisition of a Langmuir probe I-V characteristic curve is usually performed by inserting a metal tip in the plasma, and smoothly sweeping the probe bias voltage while recording the current [8–12]. In order to obtain the temporal evolution of a LP I-V curve, the voltage frequency sweep has to be much larger than the typical frequency of the observed phenomenon or process. According to waveform displayed in Fig 3, the sampling frequency must be above 1 MHz in this study, which makes measurements extremely complicated from a technical viewpoint [13, 14]. Moreover, the evolution of a vacuum arc is fast and stochastic [15], which makes data treatment and analysis challenging. An alternative method is then proposed in section IV.A to properly recover the change in time of the probe I-V curve in the course of the VAT discharge [16].

The probe was here a cylindrical tungsten LP, 0.6 mm in diameter and 14 mm in length. The probe was placed at various fixed distances from the PJP anode plane: 20 cm, 25 cm and 30 cm. Bias voltage has gradually been increased from -60 V to 60 V with 0.1 V steps using a Tenma 72-13360 power supply. The current collected by the probe was measured with a 50 Ω Pearson 2878 current probe indicating an output ratio of 0.1 V/A.

The LP measurements were complemented with Faraday cup (FC) measurements. When negatively biased, the latter allow to estimate the ion current density at a given point in the plume. The FC is composed of a conductive tube and a collector, forming a cup of which the external surface is protected from the plasma with a housing. A FC permits to neglect the edge effects coming from the sheath formation, due to its closed geometry [17]. Moreover, it mostly captures charged particles with a velocity vector parallel to the axis of alignment. The FC here presented a 15 mm cup diameter for 20 mm length, no collimator was mounted in that configuration. The cup was assembled from a molybdenum disk collector and a stainless steel tube. It has been biased with a TTI EX752M power supply. The collected current has been measured by means of an other 50 Ω Pearson 2878 current probe (0.1 V/A output ratio).

2. Time-of-Flight

Whereas the LP gives information on the electron properties in the plume, the FC indicates the ion current. An other interesting quantity concerning ions is their velocity, which can be estimated with the Time-of-Flight (ToF) method. Time of flight is in short the measurement of the time taken by an ion to travel a given distance through in a plasma. Here, this method involves measuring the ion current with an electrostatic probe at two different locations in the plasma jet. The two probes must be identical, separated by a known distance and aligned. Moreover they must be equally biased to avoid the presence of an electric field between them. Their bias voltage should be negative to solely capture ions. As the plasma is pulsed the ion current collected by the two probes rises up and then falls back to zero. The ion velocity can then be extracted from the time shift between the two waveforms. Although the method is theoretically simple, data collection and analysis are quite hard tasks when waveforms are noisy and exhibit many peaks as it will be shown in section V.A.1.

The first probe encountered by the ions was here a grid, allowing to capture some ions while letting other pass. The gridded probe was a 47 mm in diameter disk, 1 mm thick, with 1.5 mm holes. First estimate on the plasma Debye length in the plume, based on LP measurements, indicated that its order of magnitude was between 10^{-2} mm and 10^{-1} mm. The diameter of the grid holes was then way larger than the Debye length in the plasma plume. Further downstream, the ions were collected by a 15 mm in diameter planar probe (PP). The choice of a planar geometry for the second probe has been made for the sake of simplicity. Moreover, current waveforms obtained by means of the PP showed good similarities with the ones obtained with the grid, easing then the correlation process. PPs are a bit less precise than FCs for determining the current density, due to sheath effects on the edges. Notwithstanding, it does not matter much here as the core of the analysis is based on time shifts between the waveforms, the latter being normalized during the process. Finally, a 19 mm in diameter collimator was placed upstream of the two probes in order to limit the ion flux, thus reducing the probe saturation. A schematic of the setup is presented in Fig 4.

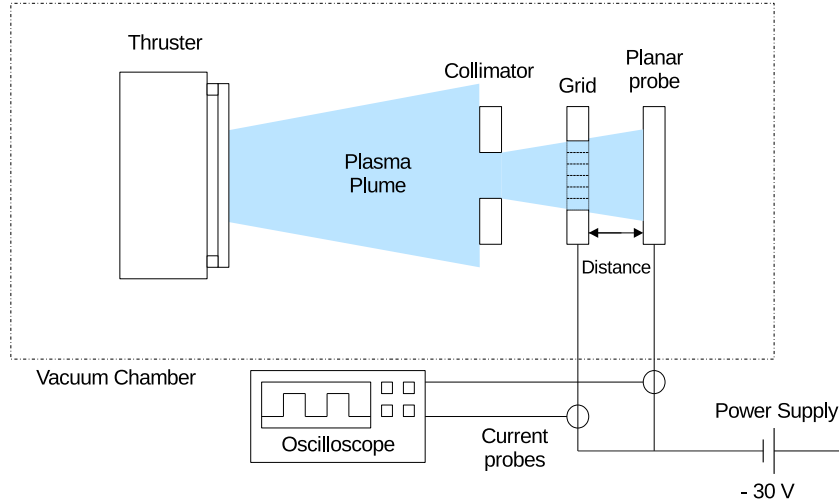


Fig. 4 Time-of-Flight experimental arrangement.

It is particularly important in that experiment that the current probes used to measure the current collected by the electrostatic probes are strictly similar. This is the reason why two $50\ \Omega$ Pearson 2878 current transformer have been placed in the circuit. The power supply used to bias both the gridded probe and the planar probe was a Tenna 72-10480.

IV. Electron properties

A. Time-resolved Langmuir Probe measurement method

The raw material of the LP analysis is the current intensity vs voltage curve (I-V curve). A voltage sweep on the probe is performed and the current to the probe is recorded. In the case of stationary plasmas, each voltage step corresponds to a constant and stable. This is due to the fact that the voltage sweep frequency is larger than the typical frequency of the observed phenomenon. Here, the plasma is pulsed and its properties change quickly as the discharge occurs only for $30\ \mu\text{s}$. An alternative method however permits to reconstruct I-V curves for each moment of the discharge. The method is based on a statistical treatment of the Langmuir probe I-V curves.

The bias voltage has gradually been increased from $-60\ \text{V}$ to $60\ \text{V}$. For each voltage step, 15 pulses were triggered and for each the probe current trace was recorded. This statistical approach allows the construction of an averaged behavior of the vacuum arc, as the discharge, hence the current waveform, varies from one pulse to another. Once all waveforms have been acquired over the selected voltage range, one only has to recover the current intensity value for a given time t on each waveform. This operation is symbolized by the dashed lines at time $t = 15\ \mu\text{s}$ and $t = 30\ \mu\text{s}$ in Fig. 5a. Once those values have been recovered, they can be plotted as a function of the voltage, allowing to reconstruct the I-V curves associated with the time t as shown in Fig 5b.

In other words, the evolution in time of the probe current for a given voltage is replaced by the change in current as a function of the applied voltage for a given time, or in short the I-V curve for a given time [16].

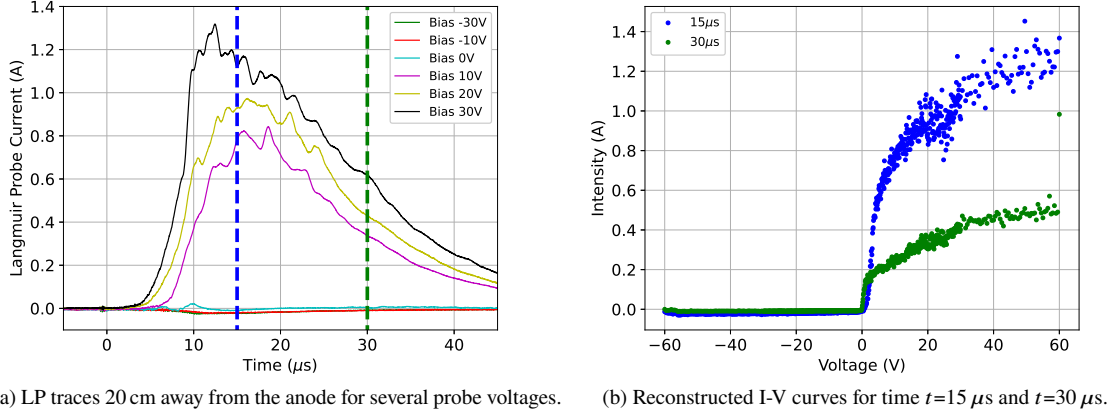


Fig. 5 I-V curve reconstruction

Once the curve is constructed, models should be applied to extract the associated physical properties. The models used in this contribution to analyze the data are the OML (Orbital Motion Limit) and the BRL (Bernstein Rabinowitz Laframboise) models. LP models and their application to various datasets are well documented [8, 16, 18–20], the objective is here neither to provide a complete tutorial on the model evaluations, nor to list all the differences between them.

Briefly, the OML model is the first ever LP analysis model. It was developed by Langmuir and Mott-Smith in 1926 [21]. This model assumes that the radius of the sheath surrounding the probe is infinite, implying that all the ions are attracted from a large distance to the probe. While being based on inaccurate assumptions, the OML proved its validity for high density plasmas [19]. This model is popular thanks to its computational simplicity leading to consistent results. Data analysis is indeed based on successive linear fits on the I-V curve, as the I_c^2 vs V slope is proportional to n_e^2 .

On the other hand, the BRL model is based on the resolution of the Poisson's equation, for the potential $V(r)$ going from the probe surface to infinity. Moreover, in this model, a Maxwellian distribution of the ion velocity is assumed. It implies that some ions can hit the probe while other can not, depending on their angular momentum. A probe absorption radius is then defined: depending on the probe potential and the ion angular momentum, some ions are trapped and collected by the probe when they cross this virtual boundary.

Differences between those two models mainly affect the evaluation of the electron density. Concerning the electron temperature, a Maxwellian distribution is assumed in both cases. The temperature is then estimated in a similar manner in OML and BRL, leading to almost no differences in the values obtained. Values of electron temperature presented in this contribution come from the evaluation of the BRL model.

Finally, the plasma potential is estimated as the maximum of dI/dV . Data being noisy in our case, a Savitzky-Golay filter as well as a 5th order spline interpolation have been applied on the I-V curves in order to compute the derivative.

B. Evolution along the axis

1. Electron density

Fig. 6 shows the temporal evolution of the electron density during a PJP current pulse computed by means of the OML model. The evolution recovered through the BRL model is shown in Fig. 7. In the early moments of the acquisition, the measured Langmuir probe current is very weak and extremely noisy, especially for the ion branch of the I-V curve. We therefore decided not to account for the data before $5 \mu s$, $6 \mu s$ or $8 \mu s$, depending on the probe-anode distance, to avoid misinterpretation. In a same way, models have not been evaluated for data after $50 \mu s$ due to a too low signal. As a matter of fact it can be seen in both figures that around $40 \mu s$ the data becomes scattered.

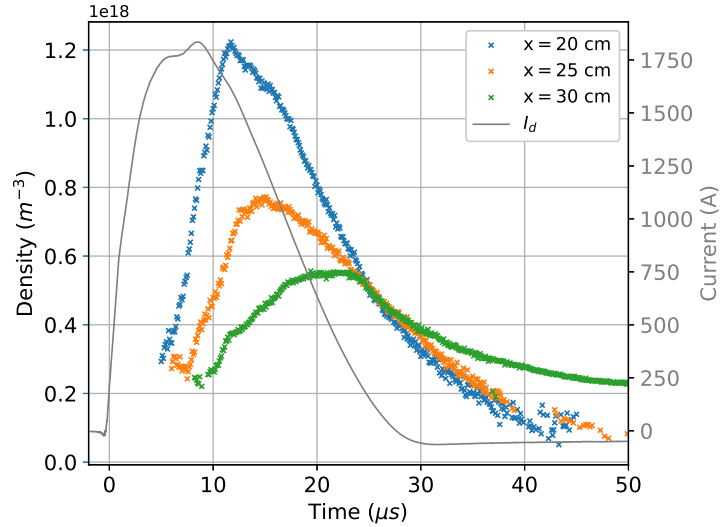


Fig. 6 Evolution of the electron density along the PJP centerline according to the OML model.

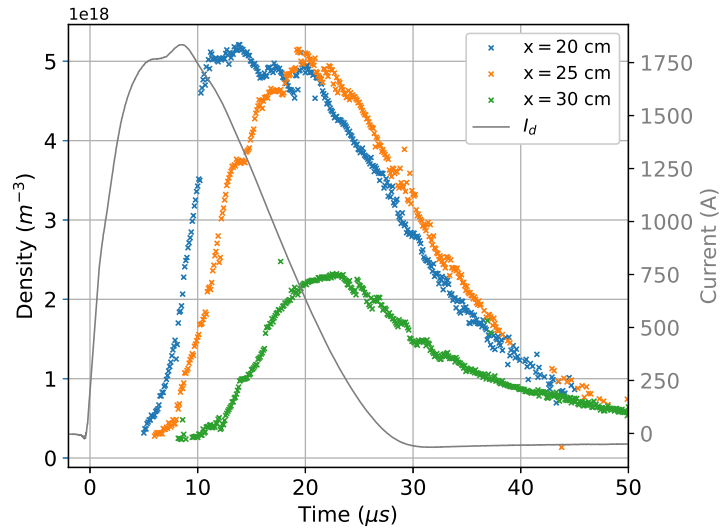


Fig. 7 Evolution of the electron density along the PJP centerline according to the BRL model.

According to the two models, the electron density evolution roughly follows the discharge current waveform. Curves obtained with the OML are nevertheless smoother than the BRL ones, especially when n_e reaches its maximum value. Furthermore, the maximum values are different from a model to the other: $1.2 \times 10^{18} \text{ m}^{-3}$ for OML and $1.2 \times 10^{18} \text{ m}^{-3}$ for BRL at $x = 20 \text{ cm}$. This discrepancy is natural as the two models differs in terms of assumptions. Moreover, it has been observed in [18] that the BRL theory tends to slightly overestimate the electron density. In any way, one can note that the plume still presents a large electron density far away from the anode, which is not so surprising as the plasma is generated from a solid state material.

In Fig. 6, the variation in electron density is clearly observed from one measurement location to an other. The time shift between the traces is also well visible. In Fig. 6, however, the electron density seems to be almost the same at $x = 20 \text{ cm}$ and $x = 25 \text{ cm}$ but shifted from a few μs . According to the two models, the $x = 30 \text{ cm}$ dataset presents a slower decrease in density.

2. Electron temperature and plasma potential

Fig. 8 shows the temporal evolution of the electron temperature T_e during a PJP current pulse. At the beginning of the discharge a high electron temperature peak is noted regardless of the distance to the anode. This high-temperature peak is a direct consequence of the very high voltage applied to the VAT electrodes during the trigger phase. A large amount of energy is injected into the discharge at the beginning of the pulse as voltage applied to the trigger electrode is much larger than the one applied to the anode.

Then, no matter the location of the probe, T_e stabilizes to 0.5 eV and slowly decreases without any apparent oscillation. The blank spaces in the curve are linked to the fact that the T_e computation algorithm is very sensitive to noise. It may happen, for noisy I-V curves, that the algorithm can not converge. This problem occurs mostly before 10 μs , during the trigger phase where the I-V curves are the noisiest.

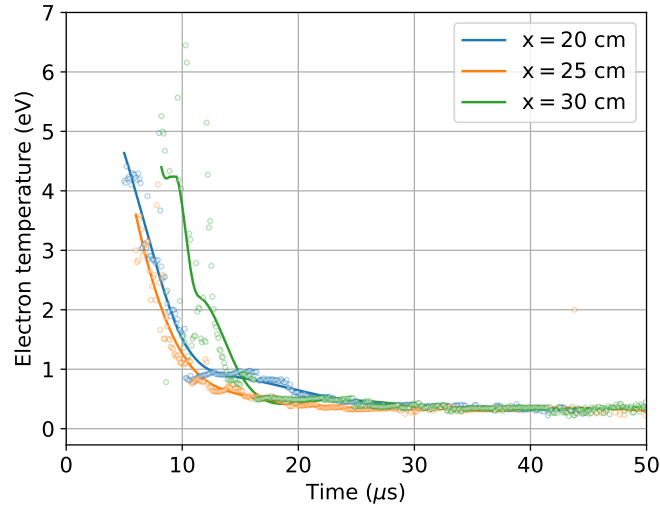


Fig. 8 Evolution of the electron temperature along the PJP centerline.

The time evolution of the plasma potential V_p is shown in Fig. 9. As expected, there are striking similarities between the temporal evolution of the plasma potential and the temporal evolution of the electron temperature. A peak of high plasma potential is observed at the beginning of the discharge, then it decreases and reaches zero. The height of this peak decreases when the probe is placed further away from the anode plane.

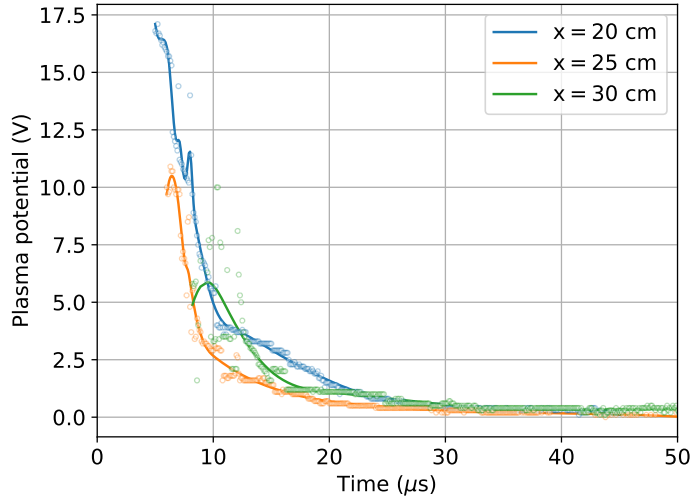


Fig. 9 Evolution of the plasma potential along the PJP centerline.

V. Investigation of ion properties

A. Velocity

1. Approach and complexity

As explained in Section III.C.2, the approach relies on the analysis of the time difference between signals collected by two probes. The probes being separated by a known distance, the velocity can be recovered. In order to get an accurate representation of the velocity distribution it is necessary to identify the different ion populations and determine their respective velocity. A peak to peak ToF data analysis algorithm has been developed to automatically process all the ion current waveforms, allowing to make statistics on a representative sample. Firstly, the main peaks that make up the waveform captured by the first probe are identified. Secondly, the corresponding peaks are identified on the second waveforms and the time difference is computed. The core of the algorithm is the `signal.find_peaks` function from the SciPy library (Python). This function takes an array and finds its local maxima by comparison of neighboring values [22]. This function is of great interest in our case as it permits to detect peaks according to different properties input by the user, such as the peak width, height, distance, and so on.

Fig. 10 shows typical traces recorded by ToF during a PJP discharge. the peaks found by the algorithm we developed are also indicated. It can be observed that ion current traces are quite irregular with a Ti cathode with peaks that are often overlap partly. The traces sometimes contain more than 4 peaks, that means more than 4 main ion populations. In that context, the user supervision for the proper functioning of the algorithm is essential during the processing of a representative sample. 30 traces are plotted, visually checked and the input parameters of the `find_peaks` function are adjusted.

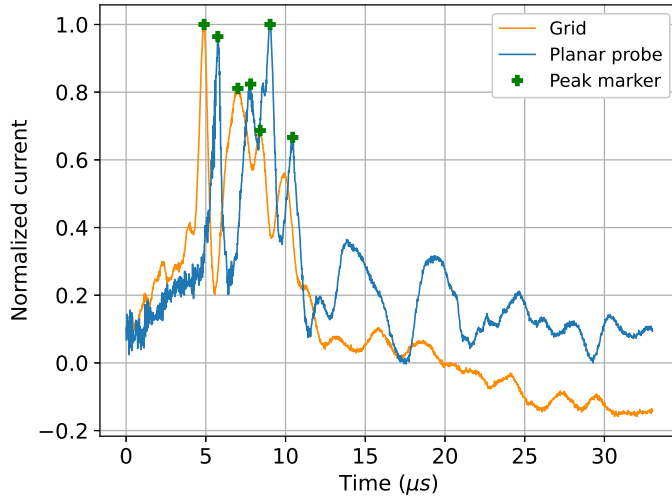


Fig. 10 Typical ion current trace obtained by means of ToF.

Once the optimal parameters have been found, the algorithm can be run autonomously on the whole dataset containing traces from 100 discharges. Fig. 11a indicates the velocity distribution of the first ion population for the range 20.8 cm to 26.1 cm from the anode. Colors on the histogram are here just an aesthetic choice to ease the visualization of each bar magnitude. The first ion population has a mean velocity of 55 km/s with a 22 km/s standard deviation. The rather high standard deviation exemplifies the uniqueness of each arc, making it necessary to acquire data over a very large number of pulses to extract a global behavior. Most of the values are contained between 40 km/s and 80 km/s which is higher than the values usually found in the literature for titanium [23].

The second population (Fig. 11b) has a mean velocity of 40 km/s with a standard deviation of 24 km/s. Velocities between 10 km/s and 20 km/s are most likely due to errors in the detection algorithm. As a matter of fact, most velocities are grouped between 30 km/s and 100 km/s. This suspected error on the second peak does however not call into question the reliability of the algorithm on the first peak. Indeed, the latter is often the one of greatest intensity, easing its identification via the algorithm.

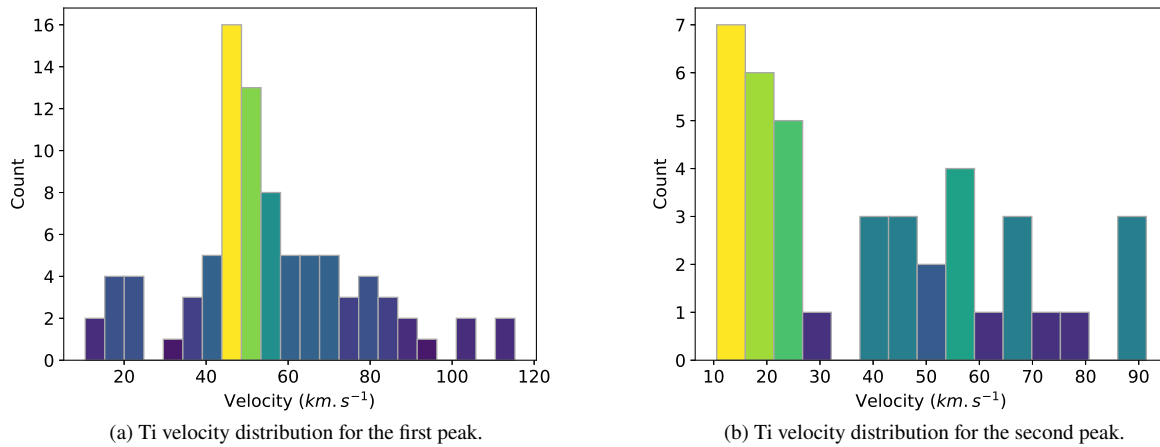


Fig. 11 Ti velocity distribution on the first two ion populations (range 20.8-26.1 cm).

2. Evolution along the centerline

The ToF setup has then been moved along the PJP centerline to measure the evolution of the ion velocity as function of the distance to the thruster. In this way, a better view of the ion velocities in the plume can be obtained. Fig. 12 shows the mean Ti ion velocity evolution in the plume. For the sake of clarity ranges of study are represented here with points, of which the x value corresponds to the middle of the distance between the two probes. It is noticed that the first ion population is systematically faster than the second population, which itself is faster than the third one. Mean velocities of the first population are between 49 km/s and 55 km/s, whereas the second population velocity ranges from 38 km/s to 47 km/s. Mean velocities on this graph and their associated standard deviation are given in Tab. 2. Values for the second and third population are given for reference, as they present a large standard deviation.

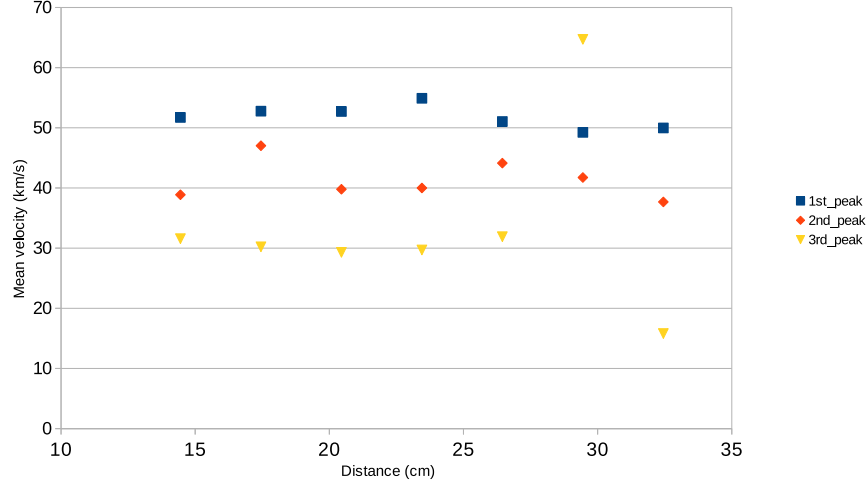


Fig. 12 Evolution of the Ti ion velocities along the PJP centerline.

Table 2 Mean Ti velocities and their associated standard deviation for different positions in the plume.

\bar{x} (cm)	\bar{v}_1 (km/s)	σ_1	\bar{v}_2 (km/s)	σ_2	\bar{v}_3 (km/s)	σ_3
14.5	52	19	39	17	32	14
17.5	53	27	47	34	30	32
20.5	53	19	38	29	29	28
23.5	55	22	40	24	30	33
26.5	51	19	44	26	32	27
29.5	49	12	42	21	65	2
32.5	50	15	38	21	16	7

First, and as previously mentioned, the mean ion velocity in the jet of the PJP shows higher values than what is usually found in the literature [23]. In this way, it appears that the Titanium ion kinetic energy in the plume is approximately 660 eV in average for the first population and 420 eV for the second one. It can be explained by the fact that the discharge current is much higher here than in most experimental arrangements set to study vacuum arcs. The energy released by the capacitors in the circuit, thus into the plasma, is here of several Joules. The correlation between the increase of discharge current and the increase of the ion velocity has already been observed for lower current vacuum arcs in [24]. Second, the first ion population is on average systematically faster than the second. Exceptions can be found for some pulses, but in the overwhelming majority of cases the first population is the fastest. As the pulse goes on, metal evaporation from macroparticles and hot craters fills the inter-electrode gap with neutrals [24, 25]. Ions created late during the pulse have then more chance to collide with neutrals, reducing their velocity. We can add to that the decrease of energy injected into the discharge linked with the decrease of the discharge current. It seems then quite consistent that the ion populations appearing late during the discharge are slower when they hit the ToF system.

In the end, no significant spatial evolution of the ion velocity is observed. This indicates that the acceleration process takes place upstream of the region studied in this work. Below 10 cm, the ion flux was too high thus saturating the probes, making data acquisition impossible with the current ToF setup. The PJP plume near field region has therefore not been investigated in this study.

B. Ion mean charge

Combining all data, one can compute the evolution in time of the ion mean electrical charge. The relation between the ion current density j_i , the plasma density n_e , the ion velocity v_i and the mean charge Q reads:

$$j_i = n_e v_i e Q \quad (1)$$

where e is the elementary charge [26]. The plasma is here assumed to be quasi-neutral with $n_e = n_i$, which can safely be considered far from the cathode surface [27, 28]. The current density was measured with a Faraday cup, with measurement averaged over 200 discharge current pulses. The electron density was inferred from Langmuir probe measurements and the ion velocity is obtained with the ToF technique. Since the different ion populations show a different velocity, and that this velocity do not seem to vary too much along the axis, v_i has been defined as the averaged velocity of the first and second peak over the entire measuring range. The velocity so obtained is then 46.5 km/s. The temporal evolution of the ion mean charge Q at $x = 20$ cm, $x = 25$ cm and $x = 30$ cm is given in Fig. 13 with values of n_e coming from the OML evaluation. Fig. 14 represents the evolution of the ion mean charge as well, recovered with values of n_e coming from the evaluation of the BRL model.

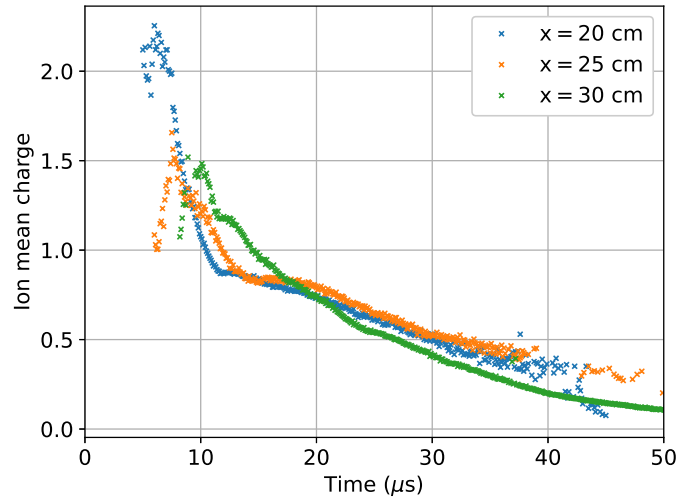


Fig. 13 Evolution of the ion mean charge along the PJP centerline (values of n_e recovered with OML).

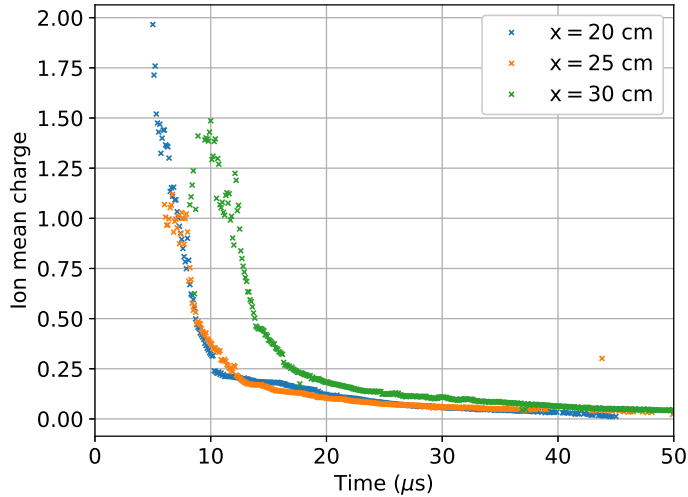


Fig. 14 Evolution of the ion mean charge along the PJP centerline (values of n_e recovered with BRL).

At ignition, the plasma contains ions with a higher charge than later during the discharge. This first regime is characterized by a high voltage and a short duration, this regime is known as the spark regime. It is known that in this specific regime ions can reach a very high charge state [4, 29]. In the case of high current sparks, the self-induced magnetic field pinches and heats the plasma. Instabilities and contractions develop in these regions of pinch, which leads to the formation of highly charged ions [30]. Ion with charged state above 10+ have indeed been observed in high current platinum vacuum spark, 20cm away from the ion source [31, 32]. It can be seen in Fig. 13 and Fig. 14 that the Titanium ion mean charge during the spark seems to be around 2+ at its highest, but most probably around 1.25+ during the spark regime. Note that the first ionization energy for Titanium is 6.82 eV.

The spark regime then gives way to the arc regime, which is characterized by a lower voltage and a relatively steady state. Regardless of the model here, the mean charge below 1+ means that the plasma is weakly ionized, and probably mostly composed of neutrals. It can be noted that for the values extracted from the BRL, the ion charge decreases much more rapidly. One should however keep in mind that values are determined here with a very simple model that rests upon several strong assumptions like an homogeneous and isotropic plasma, which is most likely not the case.

VI. CONCLUSION

Time-resolved electrostatic probe measurements performed in the jet of a pulsed high-current low-power VAT with a Ti cathode give new insights into the electrons and ions dynamics. Data inferred from LP analysis shows that the PJP operates in two distinct plasma regimes: the spark and the arc. The high-voltage discharge triggering produces a vacuum spark containing hot electrons with T_e above 4 eV as well as doubly charged ions. After ignition, the vacuum arc operates in a relatively stable regime for more than 25 μs , leading to a dense plasma plume with n_e up to 10^{18} m^{-3} 20 cm away from the anode on thruster axis. Data obtained with the Time-of-Flight method reveals ions with a higher velocity than what is usually found in the literature for similar experimental arrangements.

Measurements finally show that the evolution of the density in the plume follows fairly accurately the discharge current waveform. From that outcome one can deduce that in order to maximize the thrust, the discharge duration should be maximized as well. Nevertheless, ToF measurements reveal that ion populations appearing later during the discharge are slower. Indeed, the instantaneous energy decreases at the end of the discharge. Moreover neutrals fill the inter-electrode gap as the discharge occurs, increasing the collisions and slowing down the ions. The PJP duty cycle should be optimized too, so that the cathode could cool down and that the neutral do not fill the gap too quickly. A balance should then be found to maximize the thrust. The presence of these neutrals is also problematic with respect to the pollution of the insulator separating the triggering system and the cathode. As a metallic deposit forms on the porous surface of the insulator, the ignition becomes more difficult and the deposit sometimes even prevent the arc from occurring, reducing the lifetime of the PJP.

Acknowledgments

The research leading to these results received funding from the European Union's Horizon 2020 research and innovation program under grant agreement n° 870444 (Plasma Jet Pack).

References

- [1] Keidar, M., Schein, J., Wilson, K., Gerhan, A., Au, M., Tang, B., Idzkowski, L., Krishnan, M., and Beilis, I., "Magnetically enhanced vacuum arc thruster," *Plasma Sources Science and Technology*, Vol. 14, No. 4, 2005, p. 661.
- [2] Kolbeck, J., Anders, A., Beilis, I., and Keidar, M., "Micro-propulsion based on vacuum arcs," *Journal of Applied Physics*, Vol. 125, No. 22, 2019, p. 220902.
- [3] Polk, J., Sekerak, M., Ziemer, J., Schein, J., Qi, N., and Anders, A., "A theoretical analysis of vacuum arc thruster and vacuum arc ion thruster performance," *IEEE Transactions on Plasma Science*, Vol. 36, No. 5, 2008, pp. 2167–2179.
- [4] Michaux, E., Mazouffre, S., and Blanchet, A., "Time-evolution of plasma parameters in the jet of a low-power vacuum arc thruster," *to appear in Journal of Electric Propulsion*, 2022.
- [5] Mesyats, G., "Ecton or electron avalanche from metal," *Physics-Uspokhi*, Vol. 38, No. 6, 1995, p. 567.
- [6] Alpert, D., Lee, D., Lyman, E., and Tomaschke, H., "Initiation of electrical breakdown in ultrahigh vacuum," *Journal of Vacuum Science and Technology*, Vol. 1, No. 2, 1964, pp. 35–50.
- [7] Mazouffre, S., Michaux, E., and Vinci, A., "VAT discharge picture," *International Low Temperature Plasma Community*, Vol. Newsletter 21, March 2022, p. 2.
- [8] Chen, F., "Langmuir probe diagnostics," *Mini-Course on Plasma Diagnostics, IEEEICOPS meeting, Jeju, Korea*, 2003.
- [9] Hutchinson, I., "Principles of plasma diagnostics," *Plasma Physics and Controlled Fusion*, Vol. 44, No. 12, 2002, p. 2603.
- [10] Demidov, V., Ratynskaia, S. V., and Rypdal, K., "Electric probes for plasmas: The link between theory and instrument," *Review of scientific instruments*, Vol. 73, No. 10, 2002, pp. 3409–3439.
- [11] Merlino, R., "Understanding Langmuir probe current-voltage characteristics," *American Journal of Physics*, Vol. 75, No. 12, 2007, pp. 1078–1085.
- [12] Godyak, V., and Alexandrovich, B., "Comparative analyses of plasma probe diagnostics techniques," *Journal of Applied Physics*, Vol. 118, No. 23, 2015, p. 233302.
- [13] Pajdarová, A., Vlček, J., Kudláček, P., and Lukáš, J., "Electron energy distributions and plasma parameters in high-power pulsed magnetron sputtering discharges," *Plasma Sources Science and Technology*, Vol. 18, No. 2, 2009, p. 025008.
- [14] Dean, A., Smith, D., and Plumb, I., "A technique for recording Langmuir probe characteristics in afterglow plasmas," *Journal of Physics E: Scientific Instruments*, Vol. 5, No. 8, 1972, p. 776.
- [15] Daalder, J., "Random walk of cathode arc spots in vacuum," *Journal of Physics D: Applied Physics*, Vol. 16, No. 1, 1983, p. 17.
- [16] Dannenmayer, K., Kudrna, P., Tichý, M., and Mazouffre, S., "Measurement of plasma parameters in the far-field plume of a Hall effect thruster," *Plasma Sources Science and Technology*, Vol. 20, No. 6, 2011, p. 065012.
- [17] Hugonnaud, V., and Mazouffre, S., "Optimization of a Faraday Cup Collimator for Electric Propulsion Device Beam Study: Case of a Hall Thruster," *Applied Sciences*, Vol. 11, No. 5, 2021, p. 2419.
- [18] Chen, F., "Langmuir probe analysis for high density plasmas," *Physics of Plasmas*, Vol. 8, No. 6, 2001, pp. 3029–3041.
- [19] Chen, F., "Langmuir probes in RF plasma: surprising validity of OML theory," *Plasma Sources Science and Technology*, Vol. 18, No. 3, 2009, p. 035012.
- [20] Allen, J., "Probe theory-the orbital motion approach," *Physica Scripta*, Vol. 45, No. 5, 1992, p. 497.
- [21] Mott-Smith, H., and Langmuir, I., "The theory of collectors in gaseous discharges," *Physical review*, Vol. 28, No. 4, 1926, p. 727.

- [22] Virtanen, P., Gommers, R., Oliphant, T., Haberland, M., Reddy, T., Cournapeau, D., Burovski, E., Peterson, P., Weckesser, W., Bright, J., van der Walt, S., Brett, M., Wilson, J., Millman, K., M, N., Nelson, A., Jones, E., Kern, R., Larson, E., Carey, C., Polat, İ., Feng, Y., Moore, E., VanderPlas, J., Laxalde, D., Perktold, J., Cimrman, R., Henriksen, I., Quintero, E., Harris, C., Archibald, A., Ribeiro, A., Pedregosa, F., van Mulbregt, P., and SciPy 1.0 Contributors, “SciPy 1.0: Fundamental Algorithms for Scientific Computing in Python,” *Nature Methods*, Vol. 17, 2020, pp. 261–272.
- [23] Yushkov, G., Anders, A., Oks, E., and Brown, I., “Ion velocities in vacuum arc plasmas,” *Journal of Applied Physics*, Vol. 88, No. 10, 2000, pp. 5618–5622.
- [24] Hohenbild, S., Grübel, C., Yushkov, G., Oks, E., and Anders, A., “A study of vacuum arc ion velocities using a linear set of probes,” *Journal of Physics D: Applied Physics*, Vol. 41, No. 20, 2008, p. 205210.
- [25] Anders, A., Oks, E., and Yushkov, G., “Production of neutrals and their effects on the ion charge states in cathodic vacuum arc plasmas,” *Journal of Applied Physics*, Vol. 102, No. 4, 2007, p. 043303.
- [26] Goebel, D., and Katz, I., *Fundamentals of electric propulsion: ion and Hall thrusters*, John Wiley & Sons, 2008.
- [27] Beilis, I., “The vacuum arc cathode spot and plasma jet: Physical model and mathematical description,” *Contributions to Plasma Physics*, Vol. 43, No. 3-4, 2003, pp. 224–236.
- [28] Beilis, I., “Vacuum arc cathode spot theory: history and evolution of the mechanisms,” *IEEE Transactions on Plasma Science*, Vol. 47, No. 8, 2019, pp. 3412–3433.
- [29] Yushkov, G., and Anders, A., “Extractable, elevated ion charge states in the transition regime from vacuum sparks to high current vacuum arcs,” *Applied Physics Letters*, Vol. 92, No. 4, 2008, p. 041502.
- [30] Koshelev, K., and Pereira, N., “Plasma points and radiative collapse in vacuum sparks,” *Journal of applied physics*, Vol. 69, No. 10, 1991, pp. R21–R44.
- [31] Yushkov, G., Anders, A., Frolova, V., Nikolaev, A., Oks, E., and Vodopyanov, A., “Plasma of vacuum discharges: The pursuit of elevating metal Ion charge states, including a recent record of producing Bi 13+,” *IEEE Transactions on Plasma Science*, Vol. 43, No. 8, 2015, pp. 2310–2317.
- [32] Yushkov, G., and Anders, A., “Physical limits for high ion charge states in pulsed discharges in vacuum,” *Journal of Applied Physics*, Vol. 105, No. 4, 2009, p. 043303.